3752 *Chem. Mater.* **2009,** *21,* 3752–3762
DOI:10.1021/cm900601k

CHEMISTRY OF MATERIALS
Article

Synthesis, Characterization, and Growth Mechanism of n-Type $CuInS_2$ Colloidal Particles

Fabrice M. Courtel,[†] Royston W. Paynter,[†] Benoît Marsan,*[,‡] and Mario Morin*[,‡]

[†]*Centre Énergie, Matériaux et Télécommunications (ÉMT), Institut National de la Recherche Scientifique (INRS), 1650 Boulevard Lionel-Boulet, Varennes, Québec J3X 1S2, Canada, and* [‡]*Département de Chimie, Université du Québec à Montréal (UQÀM), C.P. 8888, Succursale Centre-ville, Montréal, Québec H3C 3P8, Canada*

Received November 11, 2008. Revised Manuscript Received July 1, 2009

We report on the growth of $CuInS_2$ n-type semiconductive particles, prepared using a modified Czekelius's colloidal method, as well as their chemical and electrochemical properties. Solid state Raman spectroscopy revealed two crystalline phases: chalcopyrite and the so-called copper−gold phase. Increasing the annealing temperature of the particles favors the formation of the chalcopyrite phase. As shown by XPS, EDX, and ICP-AES, an excess of indium was obtained, which was greater at the surface ($CuIn_{1.45}S_{1.9}$ at 450 °C) than in the bulk ($CuIn_{1.04}S_{1.74}$ at 450 °C). UV−visible measurements showed that the n-type $CuInS_2$ possesses a direct bandgap energy of 1.45 eV. Two organic redox couples in nonaqueous media were used to perform the capacitance measurements carried out by EIS on a $CuInS_2$ film: 5-mercapto-1-methyltetrazolate (T^-)/di-5-(1-methyltetrazole) disulfide (T_2) and 5-trifluoromethyl-2-mercapto-1,3,4-thiadiazolate (G^-)/5,5′-bis(2-trifluoromethyl-1,3,4-thiadiazole) disulfide (G_2). Fermi levels of −3.95 eV and −3.64 eV and majority charge carrier densities of 4.1×10^{18} and 1.8×10^{18} cm^{-3} were determined, respectively, using these redox couples. On the basis of the $CuInS_2$/electrolyte energy level diagrams, the G^-/G_2 redox couple is expected to lead to a more efficient device (greater photocurrent and photovoltage). In situ Raman spectroscopy measurements showed that the reactivity of copper with hexamethyldisilathiane is faster than with indium. This explains the excess of indium at the surface of the $CuInS_2$ particles, as well as its n-type semiconductivity.

Introduction

Ternary compounds from the $I-III-VI_2$ family, especially $CuInSe_2$ and $CuInS_2$, have been considered for photovoltaic applications because of their interesting optical properties.[1] Depending of the Cu/In ratio, they display an n-type (Cu/In < 1) or a p-type (Cu/In > 1) semiconductivity. $CuInS_2$ has a favorable direct bandgap energy of 1.5 eV[2] (827 nm), with matches closely the solar spectrum, and an absorption coefficient of 10^5 cm^{-1} (at 730−750 nm)[3] that is about 10 times greater than that of CdTe.[4] Furthermore, $CuInS_2$ is less toxic than $CuInSe_2$.

Meese et al. suggested that $CuInS_2$ has a theoretical conversion efficiency up to 30%,[5] making it an interesting semiconductor for photovoltaic applications. $CuInS_2$ is mainly used in solid−solid photovoltaic cells, such as Mo|$CuInS_2$|CdS|ZnO, which provide an efficiency of about 10%.[6,7] Commonly, this type of device can achieve a maximum efficiency of about 20% for laboratory scale cells.[1] p-type $CuInS_2$, obtained by atomic layer chemical vapor deposition (AL-CVD), has been used to prepare SnO_2:F|TiO_2|Al_2O_3|In_2S_3|$CuInS_2$|Au 3D nanocomposite solar cells, which achieve an energy conversion efficiency of 4%;[8] this is twice the performance of the best inorganic 3D solar cell reported to date. In this cell, Al_2O_3 and In_2S_3 play the role of tunnel barrier and buffer layer, respectively.

$CuInS_2$ can also be used in photoelectrochemical devices in which the semiconductor is in contact with a solution containing a redox couple.[9] One advantage of such a device is the easy formation of the semiconductor/electrolyte junction. Furthermore, there is also the possibility of using various redox couples with different standard potentials and different electron transfer kinetics,

*Corresponding authors. B.M.: phone +1 514 987-3000 ext. 7980; fax +1 514 987-4054; e-mail marsan.benoit@uqam.ca. M.M.: phone +1 514 987-3000 ext. 8239; fax +1 514 987-4054; e-mail morin.mario@uqam.ca.

(1) Lewerenz, H. J. *Sol. Energy Mater. Sol. Cells* **2004**, *83*(4), 395–407.
(2) Moller, H. J. *Semiconductors for solar cells;* Artech House Edition: Boston, 1993.
(3) Krunks, M.; Bijakina, O.; Varema, T.; Mikli, V.; Mellikov, E. *Thin Solid Films* **1999**, *338*(1−2), 125–130.
(4) Mitchell, K.; Fahrenbruch, A. L.; Bube, R. H. *J. Appl. Phys.* **1977**, *48*(2), 829–830.
(5) Meese, J. M.; Manthuruthil, J. C.; Locker, D. R. *B. Am. Phys. Soc.* **1975**, *20*, 696–703.
(6) Klaer, J.; Siemer, K.; Luck, I.; Braunig, D. *Thin Solid Films* **2001**, *387*(1−2), 169–171.
(7) Unold, T.; Sieber, I.; Ellmer, K. *Appl. Phys. Lett.* **2006**, *88*(21), 13502–13504.
(8) Nanu, M.; Schoonman, J.; Goossens, A. *Adv. Mater.* **2004**, *16*(5), 453–456.
(9) Marsan, B. Cellules photovoltaïques électrochimiques à électrolyte polymère de configuration n-CdSe//POE modifié-M2S/xS//ITO. Ph.D. Thesis, Université du Québec - Institut National de la Recherche Scientifique, Varennes-Montréal, Canada, 1988.

Published on Web 07/29/2009

in conjunction with the semiconductor material. This yields variable device photopotentials and variable device photocurrents, respectively. In this cell configuration, using an n-type $CuInS_2$ material, an efficiency of 9.7% has already been achieved using an HCl aqueous solution containing the I^-/I_3^- redox couple.[1,10] These promising results have led to an increase in the number of studies regarding the indium-rich region of the phase diagram of $CuInS_2$ where n-type semiconductivity occurs.[1]

Several synthesis methods of $CuInS_2$ have been reported, such as RF sputtering,[11,12] reactive magnetron sputtering,[7] flash evaporation,[13] electrodeposition,[14−17] single- and double-source evaporation,[18,19] chemical spray pyrolysis,[20−25] molecular beam epitaxy,[26] and heat treatment of Cu−In alloys[27] or of $Cu_2In_2O_5$[28] in H_2S. Most of these methods yield $CuInS_2$ with p-type semiconductivity. Few colloidal methods reported in the literature, using triphenyl phosphite (with hexamethyldisilathiane as a sulfur source)[29,30] or hexanethiol[31] as ligands, gave n-type $CuInS_2$. One difficulty in the synthesis of ternary materials, such as $CuInS_2$, is the control of stoichiometry. This is related to the fact that numerous crystalline phases have been reported for this material: chalcopyrite (CH), spharelite, zinc-blend, copper−gold (CuAu), and copper−platinum (CuPt).[32,33] Although these methods report in detail the optical, electrochemical, and structural properties of these particles, few address the mechanism by which they are made. Such insight into why some methods yield n-type (excess of indium) or p-type (excess of copper) would be useful for the development of colloidal synthetic methods.

In this article, we thus report on the growth mechanism of $CuInS_2$ particles obtained using Czekelius's reported synthesis method, which provides n-type $CuInS_2$ particles.[29,30] The chemical and physical properties of the particles are first presented for the bulk and the surface of the $CuInS_2$ particles. Then, electrochemical impedance spectroscopy measurements are described and analyzed to elucidate the electrical properties (type of semiconductivity, flatband potential, and majority charge carrier density) of films made of these semiconductor particles. This allows the establishment of $CuInS_2$/electrolyte energy level diagram, which is of great interest to the development of photoelectrochemical devices. Finally, this work mainly aims at bringing insights into the formation mechanism of $CuInS_2$ particles. To address this question, in situ Raman spectroscopy measurements are performed to follow the growth of the $CuInS_2$ particles. From these measurements, a growth mechanism of the particles is proposed.

Experimental Methods

Materials. Except for tetra-*n*-butylammonium perchlorate, all chemicals were used as received. $InCl_3$ (anhydrous, 99.999%), CuI (99.999%), $(CH_3)_3-Si-S-Si-(CH_3)_3$ (hexamethyldisilathiane, purum grade), $P(O-Ph)_3$ (triphenyl phosphite, TPP, 97%), CH_3CN (anhydrous, 99.8%), 1-methyl-2-pyrrolidinone (NMP, 99+%, HPLC grade), polyvinylidene fluoride (PVDF, $M_w \sim 534\,000$ g mol^{-1}), $AgNO_3$ (>99%), $AgSO_3CF_3$ (99%), ferrocene (98%), ethylene carbonate (EC, 98%), and dimethyl carbonate (DMC, ReagentPlus, 99%) were purchased from Aldrich. Tetra-*n*-butylammonium perchlorate (TBAP, 99+%, recrystallized in ethyl acetate) was obtained from Alfa Aesar. Ethanol (100%, HPLC grade) and hexane (HPLC grade) were supplied by A&C and EMD, respectively. Argon (99.6%) was purchased from Praxair. The first redox couple used for the electrochemical characterization of the semiconductor is T^-/T_2, where T^- stands for 5-mercapto-1-methyltetrazolate ion produced in solution from 5-mercapto-1-methyltetrazole (HT, $C_2H_4N_4S$, 98%) commercially available from Aldrich, whereas the oxidized species di-5-(1-methyltetrazole) disulfide (T_2) was synthesized using a procedure described elsewhere.[34] The second redox couple is G^-/G_2, where G^- stands for 5-trifluoromethyl-2-mercapto-1,3,4-thiadiazolate ion produced in solution from the potassium salt KG and the oxidized species G_2 for 5,5′-bis(2-trifluoromethyl-1,3,4-thiadiazole) disulfide. KG and G_2 were synthesized using a procedure

(10) Goslowsky, H.; Fiechter, S.; Konenkamp, R.; Lewerenz, H. J. *Sol. Energy Mater.* **1986**, *13*(3), 221–232.
(11) Watanabe, T.; Matsui, M.; Mori, K. *Sol. Energy Mater. Sol. Cells* **1994**, *35*(1−4), 239–245.
(12) Hwang, H. L.; Cheng, C. L.; Liu, L. M.; Liu, Y. C.; Sun, C. Y. *Thin Solid Films* **1980**, *67*(1), 83–94.
(13) Agarwal, M. K.; Patel, P.; Chaki Sunil, D. H.; Lakshminarayana, D. *Bull. Mater. Sci.* **1998**, *21*(4), 291–296.
(14) Herrero, J.; Ortega, G. *Sol. Energy Mater. Sol. Cells* **1990**, *20*(1−2), 53–65.
(15) Payment, F. Électrodéposition du semi-conducteur ternaire CuInS2 pour utilisation dans une cellule photovoltaïque électrochimique. M.Sc. Thesis, Université du Québec à Montréal, Montreal, Canada, 2003.
(16) Morin, S. Déposition galvanostatique du semi-conducteur CuInS2 sur un substrat de titane. M.Sc. Thesis, Université du Québec à Montréal, Montreal, Canada, 2006.
(17) Yukawa, T.; Kuwabara, K.; Koumoto, K. *Thin Solid Films* **1996**, *286*(1−2), 151–153.
(18) Kazmerski, L. L.; Ayyagari, M. S.; Sanborn, G. A. *J. Appl. Phys.* **1975**, *46*(11), 4865–4869.
(19) Hwang, H. L.; Lin, H. Y.; Hwang, B. H.; Wu, Y. L.; Sun, C. Y. Growth and characterization of $CuInS_2$ thin films. *Proceedings of the 5th International Photovoltaic Solar Energy Conference*; Abstract number A85-11301 02-44, Athens, Greece, October 17−21, 1983; D. Reidel Publishing Co.: Dordrecht (The Netherlands), 1984, pp 908−912.
(20) Oja, I.; Nanu, M.; Katerski, A.; Krunks, M.; Mere, A.; Raudoja, J.; Goossens, A. *Thin Solid Films* **2005**, *480*, 82–86.
(21) Bihri, H.; Abd-Lefdil, M. *Thin Solid Films* **1999**, *354*(1−2), 5–8.
(22) Krunks, M.; Kijatkina, O.; Rebane, H.; Oja, I.; Mikli, V.; Mere, A. *Thin Solid Films* **2002**, *403−404*, 71–75.
(23) Ortega-López, M.; Morales-Acevedo, A. *Thin Solid Films* **1998**, *330*(2), 96–101.
(24) John, T. T.; Wilson, K. C.; Ratheesh Kumar, P. M.; Sudha Kartha, C.; Vijayakumar, K. P.; Kashiwaba, Y.; Abe, T.; Yasuhiro, Y. *Phys. Status Solidi A* **2005**, *202*(1), 79–84.
(25) Hayre, R. O.; Nanu, M.; Schoonman, J.; Goossens, A.; Wang, Q.; Grätzel, M. *Adv. Funct. Mater.* **2006**, *16*(12), 1566–1576.
(26) White, F. R.; Clark, A. H.; Graf, M. C.; Kazmerski, L. L. *J. Appl. Phys.* **1979**, *50*(1), 544–545.
(27) Grindle, S. P.; Smith, C. W.; Mittleman, S. D. *Appl. Phys. Lett.* **1979**, *35*(1), 24–26.
(28) Wada, T.; Negami, T.; Nishitani, M. *J. Mater. Res.* **1993**, *8*, 545–550.
(29) Czekelius, C.; Hilgendorff, M.; Spanhel, L.; Bedja, I.; Lerch, M.; Müller, G.; Bloeck, U.; Su, D.-S.; Giersig, M. *Adv. Mater.* **1999**, *11*(8), 643–646.
(30) Arici, E.; Hoppe, H.; Reuning, A.; Sariciftci, N. S.; Meissner, D. In CIS Plastic Solar Cells. *Proceedings of the 17th European Photovoltaic Solar Energy Conference*; Munich, Germany, October 22−26, 2001; James and James Ltd.: London, 2001, pp 61−63.
(31) Castro, S. L.; Bailey, S. G.; Raffaelle, R. P.; Banger, K. K.; Hepp, A. F. *J. Phys. Chem. B* **2004**, *108*(33), 12429–12435.
(32) Alvarez-Garcia, J.; Barcones, B.; Perez-Rodriguez, A.; Romano-Rodriguez, A.; Morante, J. R.; Janotti, A.; Wei, S. H.; Scheer, R. *Phys. Rev. B* **2005**, *71*(054303), 1–9.
(33) Shay, J. L.; Wernick, H. *Ternary Chalcopyrite Semiconductors: Growth, Electronic Properties and Applications*; Pergamon Edition: Oxford, U.K., 1975.
(34) Philias, J. M.; Marsan, B. *Electrochim. Acta* **1999**, *44*(14), 2351–2363.

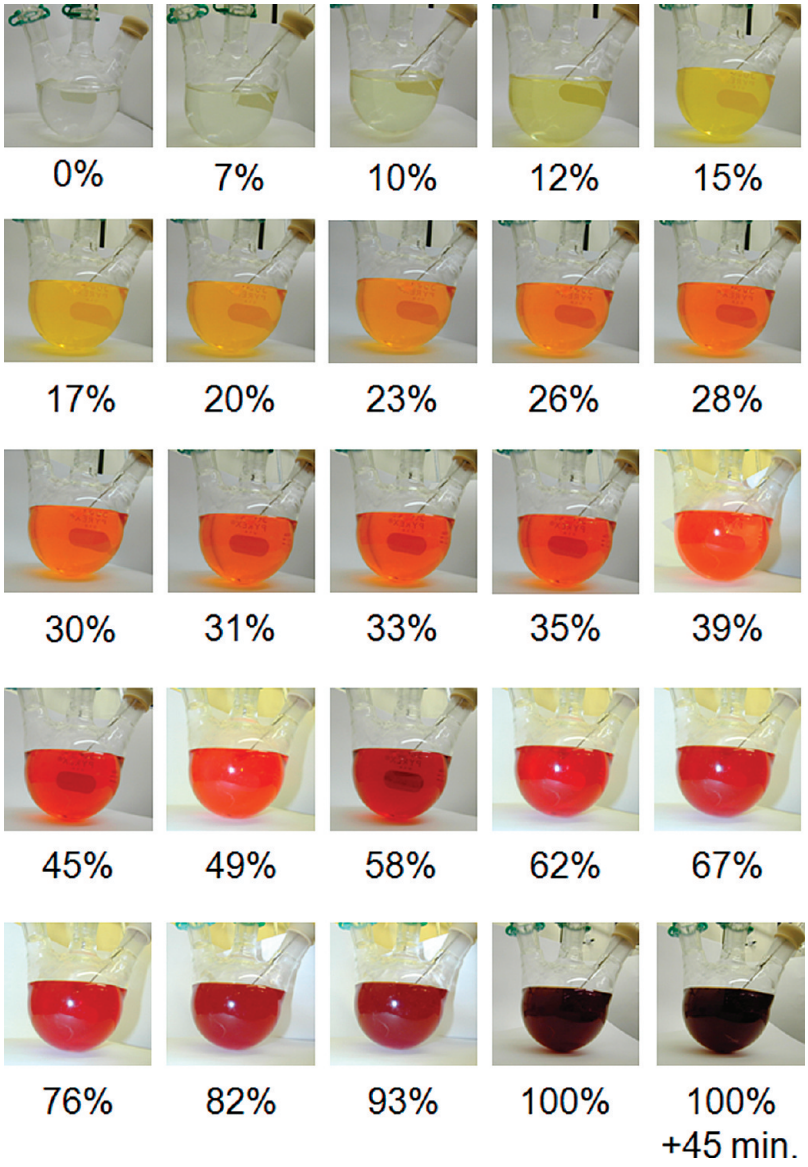

Figure 1. Photos of the color change during the addition of the hexamethyldisilathiane. The percentages represent the amount of hexamethyldisilathiane added.

developed by Hersant et al.[35,36] The structures of the redox molecules are shown in the Supporting Information S2.

Synthesis. A two-step colloidal method reported in the literature[29,30] was used for the synthesis of $CuInS_2$ particles. The method was modified as follows: the indium/TPP molar ratio was set to 1:3, instead of 1:2 (see below), and the quantity of sulfur used was twice that required for the stoichiometry of $CuInS_2$. The first step of the synthesis is the formation of metal ions complexes (Cu^+ and In^{3+}) with TPP, carried out in argon, as shown by the proposed eqs 1 and 2:

$$InCl_3 + 3P(O{-}Ph)_3 \rightarrow [In(P(O{-}Ph)_3)_3]^{3+} + 3Cl^- \quad (1)$$

$$CuI + 3P(O{-}Ph)_3 \rightarrow [Cu(P(O{-}Ph)_3)_3]^{+} + I^- \quad (2)$$

In a three-neck flask, three equivalents of TPP were added to one equivalent of $InCl_3$ in acetonitrile (0.1 M). The suspension was refluxed for 2 h while stirring, in order to form the $[In\ (TPP)_3]^{3+}$ complex. The mixture was allowed to cool to room temperature. The same procedure was used to prepare the $[Cu\ (TPP)_3]^{+}$ complex. In a second step, the above two solutions were mixed, stirred for 1 h and kept under argon. Then four equivalents of hexamethyldisilathiane were added at a rate of 0.07 mL min^{-1}, while stirring. This resulted in the formation of $CuInS_2$, as shown by the proposed Equation 3:

$$[Cu(P(O{-}Ph)_3)_3]^{+} + [In(P(O{-}Ph)_3)_3]^{3+} + 2(CH_3)_3Si{-}S{-}Si(CH_3)_3 \rightarrow CuInS_2 + 6P(O{-}Ph)_3 + 4(CH_3)_3Si^{+} \quad (3)$$

As mentioned by Czekelius et al.[29] and Arici et al.[30] during the sulphide addition, the color of the solution changed gradually from colorless to yellow, orange, red, dark red, and dark brown. The color change is shown by Figure 1. After the addition of hexamethyldisilathiane, the suspension was stirred for 2 h, and then the particles were allowed to grow for 24 h. Most of the

(35) Hersant, G. Préparation et caractérisations de nouveaux milieux électrolytiques quasi-transparents destinés à une application en pile solaire. Ph.D. Thesis, Concordia University - Université du Québec à Montréal, Montreal, Canada, 2009.
(36) Hammami, A.; Marsan, B.; Armand, M.; Hersant, G. Redox Couples, Compositions and Uses Thereof. WO 2007/109907 and CA 2,541,232, 2006 and 2007.

solvent was removed using a rotative evaporator (40 °C under vacuum). The $CuInS_2$ particles were then extensively rinsed with hexane and subsequently rinsed with a 1:1 ethanol/hexane mixture. Finally, the particles were dried at 40 °C under vacuum and stored under vacuum. To increase their crystallinity, the particles were annealed at 450 °C under vacuum (100 mTorrs), in a tubular furnace (Lindberg/Blue M, model TF55035A-1), at a heating rate of 2 °C min^{-1}. The annealing temperature was then held constant for 3 h, and then the samples were cooled to room temperature.

Characterization. The crystalline phases of the $CuInS_2$ particles were obtained from X-ray diffraction (XRD, Siemens D-5000, cobalt X-ray source, $K\alpha_1$ λ: 1.7890 Å, step size 0.02°, 2 s per step) and Raman spectroscopy (Renishaw RM 3000, λ_{ex}: 782 nm) measurements. Infrared diffuse reflectance measurements were performed using a FTIR spectrometer with a diffuse reflectance accessory (Fourier transformed infrared, Thermo Nicolet Avatar 360). The bulk stoichiometry was estimated by energy dispersive X-ray (EDX, EDAX detector integrated into the scanning electron microscope (SEM)) and inductively coupled plasma−atomic emission spectroscopy (ICP-AES, Jobin Yvon Horiba JY2000, λ_{Cu}: 223.008 nm and λ_{In}: 230.606 nm). The surface stoichiometry was determined by X-ray photoelectron spectroscopy (XPS, VG Escalab 200iXL, $\lambda_{Alachromatic}$: 1486.7 eV). Surface analysis of the particles, done by XPS, was also carried out to obtain the oxidation state of the elements and to detect surface contaminations. The bandgap energy of the $CuInS_2$ particles was determined from the UV−visible spectrum (Varian Cary 100 Bio). The crystallite size was calculated using the XRD results and the Scherrer equation with a shape factor of 0.9,[37] and the particle size was estimated using SEM (Hitachi S-4300SE/N VP-SEM).

Electrochemical impedance spectroscopy (EIS) was used to determine the type of semiconductivity, the Fermi level, and the majority charge carrier density of a $CuInS_2$ film (multipotentiostat: solartron 1470 and frequency response analyzer: solartron 1255B). A one-compartment glass electrochemical cell with a three-electrode configuration was used. The working electrode was a film of $CuInS_2$ particles with an electrochemical active surface area of 3.7 cm^2. A solution containing 98 wt % of $CuInS_2$ particles (annealed at 450 °C) and 2 wt % of PVDF dispersed in NMP was used to immobilize the particles onto an ITO conducting glass substrate (8 Ω/□). The electrode was dried, under vacuum, at 80 °C for 24 h. A 6 cm^2 platinum gauze (99.9%) served as the counter electrode, and a nonaqueous Ag/Ag^+ electrode was used as the reference. For the T^-/T_2 redox couple, the reference electrode was made of a silver wire dipped into an acetonitrile solution containing 0.01 M of $AgNO_3$ and 0.30 M of TBAP. A potential of 0.318 V with respect to the normal hydrogen electrode (NHE) was measured for this reference electrode at a platinum electrode, using a 0.025 M ferrocene solution. The electrolyte solution contained 0.10 M of HT, 0.01 M of T_2, and 0.30 M of TBAP (used as a supporting electrolyte) dissolved in acetonitrile. For the G^-/G_2 redox couple (insoluble in acetonitrile), the reference electrode was prepared using a solution of EC-DMC (50:50 (vol%/vol%)) containing 0.005 M of $AgSO_3CF_3$ and 0.30 M of TBAP. A potential of 0.745 V vs NHE was measured. The electrolyte solution contained 0.0375 M of KG and 0.0125 M of G_2, dissolved in EC-DMC with 0.30 M of TBAP. For each applied potential, the frequency of the superimposed voltage (amplitude of 10 mV) was scanned from 1 MHz to 10 Hz.

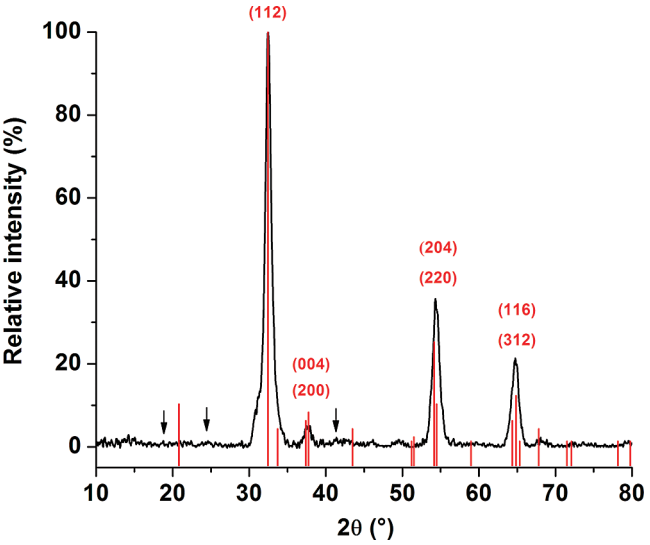

Figure 2. X-ray diffractogram of $CuInS_2$ particles annealed for 3 h at 450 °C under vacuum (100 mTorrs). Lines at the bottom of the graph come from the 27-0159 JCPDS card of the CH phase.[38] The arrows indicate the positions of low-intensity peaks associated with the CuAu phase.

Kinetics measurements, done by in situ Raman spectroscopy, were performed using two solutions of 0.0575 M of In-TPP and Cu-TPP complexes in acetonitrile. A solution of 0.1138 M of hexamethyldisilathiane in acetonitrile was used as a sulfur source and was added at a rate of 0.08 mL min^{-1}. All solutions were prepared and kept under argon during the entire experiment. A Renishaw RM 3000 Raman spectrometer coupled with a Leica optical microscope was used. Three laser wavelengths were available: 488 nm, 633 nm, and 785 nm. The latter was used for all the measurements because it gave the best signal/noise ratio at a power density of 3 mW μm^{-2}. Because the solutions were prepared in normal glass vials, identification of the Raman vibrations of glass was done ($\bar{\nu}$: 430, 448, 670, 821, 877, 900, and 1035 cm^{-1}).

Results and discussion

X-ray Diffraction and Solid State Raman Spectroscopy. Figure 2 shows the diffractogram of the $CuInS_2$ particles annealed for 3 h at 450 °C under vacuum. The chalcopyrite $CuInS_2$ phase (CH) was identified, and the peak positions are in close agreement with the JCPDS card 27-0159[38] which is shown as lines in Figure 2. The cell parameters a and c were estimated from the observed 2θ angles of the diffraction peaks (112), (204)/(220), and (116)/(312). This was done using Bragg's law and the CelRef3 software.[39] The a and c parameters are 5.51(1) and 11.143(3) Å, respectively. These values correspond well with the JCPDS card 27-0159 of the CH phase of $CuInS_2$.[38] The full width at half-maximum (fwhm) value of 0.88° for the main peak (112) is smaller than the one reported in the literature for a similar method of preparation, but without annealing: 2.94°[30] and 2.5°.[29]

(37) Golub, B. D. *Elements of X-ray Diffraction*, 2nd ed.; Addison-Wesley Publishing Inc.: Amsterdam, The Netherlands, 1978; Vol. .

(38) Hahn, H., *Powder Diffraction File of Inorganic Phases*; International Center for Diffraction Data: Swarthmore, PA, 1953; Vol. *27-0159*.

(39) Bochu, B.; Laugier, J., *CelRef*, version 3; Laboratoire des Matériaux et du Génie Physique de l'École Nationale Supérieure de Physique de Grenoble: Grenoble, France, 1987.

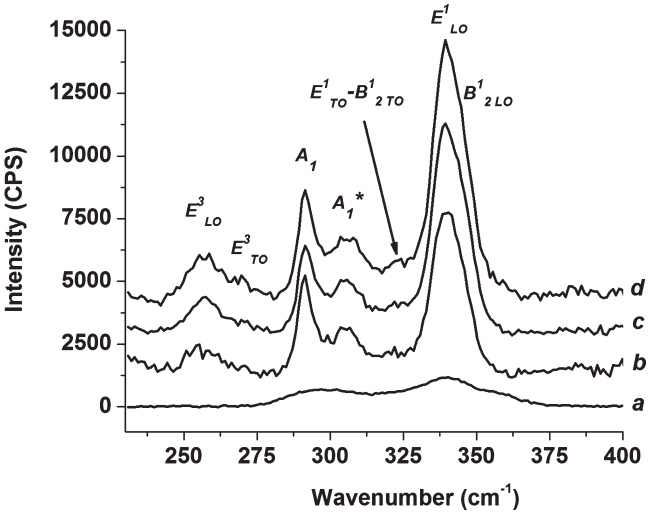

Figure 3. Raman spectra of $CuInS_2$ particles annealed for 3 h under vacuum: (a) at 300 °C; (b) at 400 °C; (c) at 450 °C; and (d) at 500 °C.

It indicates a larger crystallite size in our study: 9.3 nm when the particles were annealed at 450 °C. The method described in ref 31 uses the precursor $(PPh_3)_2CuIn(SEt)_4$; it yields a crystallite size of about 4 nm for particles annealed at 250 °C. Electrodeposition of a $CuInS_2$ film onto titanium substrate yielded particles with higher crystallinity (crystallite size of about 40 nm).[15,16] However, in those latter studies, significant surface oxidation of the particles occurred during the deposition and the subsequent annealing step (425 °C under vacuum and/or nitrogen).

Vibrational Raman spectroscopy is also used to identify the crystalline phases of $CuInS_2$. In Figure 3, eight vibrational modes are identified, peaks E^3_{LO}, E^3_{TO}, A_1, E^1_{TO}, B^1_{2TO}, E^1_{LO}, and B^1_{2LO}; they are all assigned to the CH phase,[40] whereas the A_1* peak belongs to the copper−gold (CuAu) crystalline phase.[40−42] As already reported in the literature, a mixture of two $CuInS_2$ crystalline phases is usually observed: the CH phase and the CuAu phase.[42] In Figure 2, the main diffraction peaks can be assigned to both structures. However, differences between these two structures appear at low angles. The arrows indicate the positions of these low intensity peaks (5%) associated exclusively with the CuAu phase.[40] The crystallinity of the obtained powder does not enable the XRD measurements to show the presence of these low intensity peaks, whereas Raman spectra of the powder provide clear evidence that the CuAu phase is present.

The A_1 peak corresponds to the main vibrational band related to the CH phase. This peak shifts slightly from 289 to 292 cm^{-1} with the increase of the annealing temperature from 300 to 500 °C (see Figure 3). The wavenumber of this peak is in agreement with the literature.[40,42] The A_1* peak has been first assigned to the β-In_2S_3 phase or to a $CuInS_2$ indium rich phase.[43,44] Riedle[40] and Alvarez-Garcia[42] later demonstrated that the A_1* peak is associated with the presence of the CuAu phase. A_1* peak moves from 302 to 305 cm^{-1} as the annealing temperature increases from 300 to 500 °C. The E^1_{LO} peak, at about 340 cm^{-1},[45] was first assigned to a $CuIn_5S_8$ phase,[46] but no trace of such a phase has been detected by XRD in our work. Moreover, no Raman peak at 475 cm^{-1}, indicative of Cu_xS phases,[42] was observed. With annealing temperatures going from 400 to 500 °C and using a deconvolution technique with Gaussian peaks, the A_1/A_1* ratio is kept approximately constant at 2; hence, the CH phase dominates at these temperatures. The increase of the annealing temperature favors the formation of the CH phase, which should improve the device photoconversion efficiency since the CuAu phase is known to decrease the photovoltaic effect.[40] However, the CuAu phase content seems to be greater than that of materials produced by a gas phase synthetic method.[42]

Scanning Electron Microscopy. SEM images of a film of $CuInS_2$, deposited onto an ITO glass substrate and annealed under vacuum for 3 h at 450 °C, are shown in Figure 4. It can be seen that the particle size ranges approximately from 200 to 500 nm, with some spherical particles reaching a diameter greater than 1 μm.

Infrared Spectroscopy. Infrared spectroscopy was used to verify the presence of residual organic contaminants on $CuInS_2$ particles since such contaminants might be detrimental to the performance of the solar cell. FTIR spectra of unannealed particles and particles annealed at 450 °C are shown in Figure 5. On the spectrum of the unannealed particles (Figure 5a), organic contaminants are present. Peaks observed between 2960 and 2860 cm^{-1} (CH aliphatic stretches) and at 1250 cm^{-1} (Si−CH_3 stretch) correspond to the presence of aliphatic fragments coming from hexamethyldisilathiane. The intense band at 1750 cm^{-1} is assigned to the presence of the C=O bond, coming from the oxidation of some of the organic reagents. The presence of aromatic compounds coming from TPP is shown by the two peaks between 1400 and 1500 cm^{-1}. The two other peaks between 1000 and 1100 cm^{-1} are assigned to P−O stretching modes associated with TPP. The large band at 3500 cm^{-1} comes from the adsorbed water on the powder since the measurements were done in air. As shown in Figure 5b, after annealing the particles at 450 °C under vacuum, there is a decrease of the intensity of all vibrational bands, indicating a decrease of the organic contaminants.

(40) Riedle, T. Raman Spectroscopy for the Analysis of the Thin CuInS2 Films. Ph.D. Thesis, Technical University of Berlin, Berlin, Germany, 2002.
(41) Wei, S. H.; Zhang, S. B.; Zunger, A. *Phys. Rev. B* **1999**, *59*(4), R2478–R2481.
(42) Alvarez-Garcia, J. Characterisation of CuInS2 films for solar cell applications by Raman Spectroscopy. Ph.D. Thesis, University of Barcelona, Barcelona, Spain, 2002.
(43) Morell, G.; Katiyar, R. S.; Weisz, S. Z.; Walter, T.; Schock, H. W.; Balberg, I. *Appl. Phys. Lett.* **1996**, *69*(7), 987–989.
(44) Hunger, R.; Wilhelm, M.; Diesner, K.; Bruns, J.; Lippold, G.; Hinrichs, K.; Esser, N.; Lewerenz, H. J.; Scheer, R. Phase Segregation in Epitaxial CuInS2 films. Presented at 2nd World Conference on Photovoltaic Solar Energy Conversion, Vienna (Austria), July 6−10, 1998.
(45) Rudigier, E. Phase transformations and crystalline quality of CuInS2 thin films. Ph.D. Thesis, Philipp's University of Marburg, Marburg, Germany, 2004.
(46) Rudigier, E.; Barcones, B.; Luck, I.; Jawhari-Colin, T.; Perez-Rodriguez, A.; Scheer, R. *J. Appl. Phys.* **2004**, *95*(9), 5153–5158.

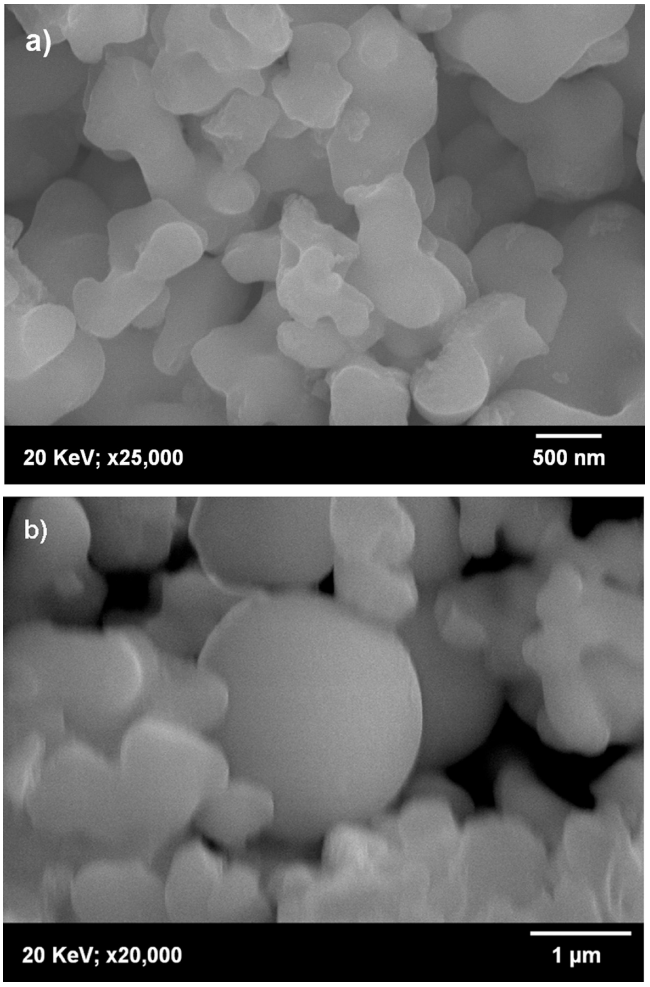

Figure 4. SEM images of a film of $CuInS_2$, deposited onto an ITO glass substrate and annealed under vacuum for 3 h at 450 °C, at a magnification of (a) 25 000× and (b) 20 000×.

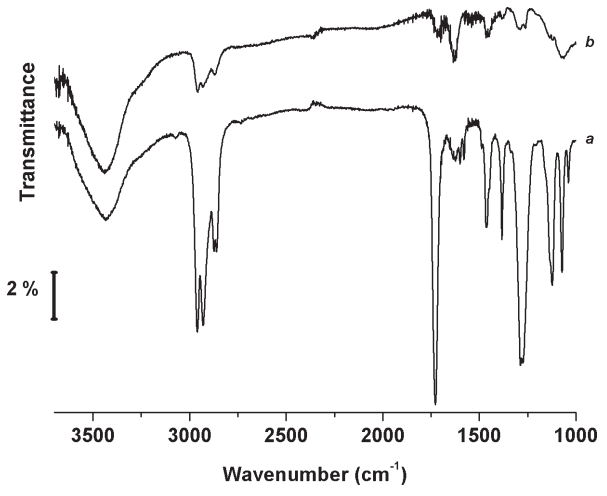

Figure 5. FTIR spectra of $CuInS_2$ particles: (a) unannealed and (b) annealed at 450 °C for 3 h under vacuum.

Bulk Stoichiometry. EDX and ICP-AES measurements were performed on annealed $CuInS_2$ particles, and the results are shown in Table 1. EDX analysis gave a Cu:In:S ratio of 1:1.04(4):1.74(7) whereas ICP-AES measurements gave a Cu:In ratio of 1:1.11(3). Both techniques have shown that the $CuInS_2$ particles synthesized in this work have an excess of indium which should lead to n-type semiconductivity.

Table 1. Stoichiometry of $CuInS_2$ Particles Obtained by EDX, ICP-AES, and XPS

	Cu	In	S
EDX	1	1.04(4)	1.74(7)
ICP-AES	1	1.11(3)	
XPS 300 °C	1	1.3(1)	1.9(1)
XPS 450 °C	1	1.5(1)	1.9(1)

X-ray Photoelectron Spectroscopy. The elemental surface composition of the $CuInS_2$ particles after thermal treatment was determined from XPS measurements (a survey spectrum is shown in Supporting Information S1). Typical XPS spectra of the most intense peaks of the three main elements (Cu $2p_{3/2}$, In $3d_{5/2}$, and S 2p) are shown in Figure 6. On Figure 6a, a single copper $2p_{3/2}$ peak, at a binding energy (BE) of 932.7(1) eV, is present. The copper Auger parameter is 1849.2 eV; it was calculated form the sum of the BE of the $2p_{3/2}$ XPS peak and the kinetic energy (KE) of the $L_3M_{45}M_{45}$ Auger peak (at 916.5(3) eV). The copper oxidation state is thus +1.[47] The indium $3d_{5/2}$ XPS peak, at a BE of 445.0(1) eV (see Figure 6b), and the indium $M_4N_{45}N_{45}$ Auger peak, at a KE of 407.0(3) eV, give an Auger parameter of 852.0 eV, which suggests that the oxidation state of indium at the surface of the $CuInS_2$ particles is +3.[47] However, the BEs of the $3d_{5/2}$ peak, when indium is bonded to sulfur or to oxygen, are very close. Nevertheless, in our case, no significant oxygen content was detected. The sulfur $2p_{3/2}$ XPS peak (see Figure 6c, right fitted peak) has a chemical shift of 161.8(1) eV, which is typical of a sulphide, that is, a sulfur bonded to copper or indium.[47] The oxidation state of sulfur at the surface of the $CuInS_2$ particles is therefore −2. Table 2 compares the peak positions of copper, indium, and sulfur orbitals. XPS peaks reported in the literature for $CuInS_2$ films prepared by noncolloidal methods[24,48] have the same BE as those measured on samples produced in this work. Small amounts (less than 5%) of phosphorus, iodine, and silicon, which come from the reactants, are also observed along with oxygen and carbon. Below 300 °C, the quantity of oxygen is stable at 4% whereas at 450 °C, it increased to 7%. The surface composition of the particles, estimated from XPS data, varies with the annealing temperature. The In/Cu ratio rises from 1.3 at 300 °C to 1.5 at 450 °C, indicating a migration of indium to the surface at higher temperature. The S/(In+Cu) ratio ranges from 0.95 (20 °C) to 0.75 (450 °C) but does not show any trend with the annealing temperature. As shown in Table 1, when the particles are annealed at 450 °C, at the surface, there is a Cu:In:S ratio of 1:1.5(1):1.9(1).

UV−Visible Spectroscopy. Optical measurements were carried out to determine the bandgap energy (E_g) of the

(47) Moulder, J. F.; Stickle, W. F.; Sobol, P. E.; Bomben, K. D. In *Handbook of X-ray Photoelectron Spectroscopy, A reference book of standard spectra for identification and interpretation of XPS data*; Chastain, J., Ed.; Perkin-Elmer Corporation: Eden Prairie, 1992.
(48) Scheer, R.; Lewerenz, H. J. *J. Vac. Sci. Technol., A* **1994**, *12*(1), 56–60.

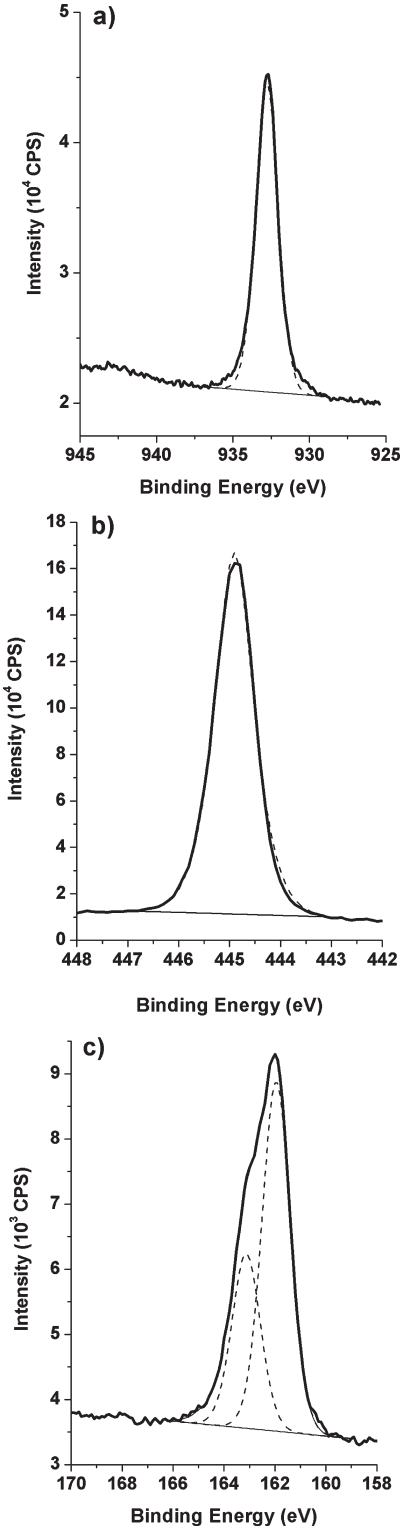

Figure 6. XPS spectra of (a) Cu $2p_{3/2}$ level, (b) In $3d_{5/2}$ level, and (c) S $2p_{3/2}$ (right fitted peak) and $2p_{1/2}$ (left fitted peak) levels of $CuInS_2$ particles annealed at 450 °C for 3 h under vacuum.

synthesized $CuInS_2$ particles annealed at 450 °C. Ten micrometer thick $CuInS_2$ films prepared onto ITO conducting glass substrates were used. Figure 7 shows the $(\alpha h\nu)^2$ vs $h\nu$ curve, where α is the absorption coefficient and $h\nu$ is the incident photon energy. The linear part of

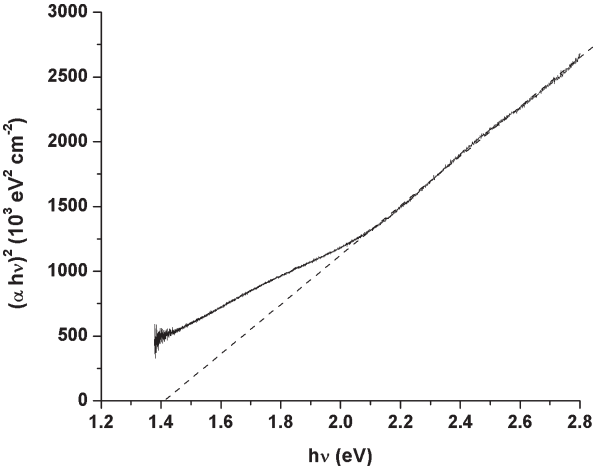

Figure 7. Plot of $(\alpha h\nu)^2$ versus photon energy ($h\nu$) for a 10 μm thick $CuInS_2$ film deposited onto an ITO conducting glass substrate. The particles were annealed at 450 °C for 3 h under vacuum.

Table 2. XPS (BE) and Auger (KE) Peak Positions Obtained for $CuInS_2$ Particles Annealed at Different Temperatures for 3 h under Vacuum (see text for detail)[a]

XPS and Auger peaks or Auger parameter	this work (20−450 °C) (eV)	refs 24, 48 (eV)
Cu $2p_{3/2}$	932.7(1)	932.2 to 932.8
Cu $L_3M_{45}M_{45}$	916.5(3)	
Cu Auger parameter	1849.2	1848.9 to 1849.1
In $3d_{5/2}$	445.0(1)	444.7 to 445.4
In $M_4N_{45}N_{45}$	407.0(3)	
In Auger parameter	852.0	852.4 to 852.6
S $2p_{3/2}$	161.8(1)	161.4 to 162.7
Cu $2p_{3/2}$−S $2p_{3/2}$	770.9(2)	770.0 to 770.2
Cu $2p_{3/2}$−In $3d_{5/2}$	487.7(2)	487.3 to 487.5

[a] BE: binding energy. KE: kinetic energy.

the curve gives a direct bandgap energy of 1.45 eV. This is in good agreement with the value of 1.5 eV reported in the literature.[29,49] The bandgap energy found in this work is very close to that of crystalline $CuInS_2$ thin films prepared from particles synthesized using a similar colloidal method.[29] Arici et al.[30] used two different conditions for measuring the visible spectra. The first measurements were performed in the reaction medium (colloidal route), and a bandgap energy of about 2.13 eV was obtained. From the absorption spectrum of a $CuInS_2$ film prepared on ZnO and sintered at 400 °C for 20 min under vacuum, a value of about 1.65 eV was obtained. The difference might be due to the absorption onset generally observed at a shorter wavelength for nanosized particles. Other synthetic methods yielded bandgap energies between 1.4 and 1.5 eV.[21]

All the analyses indicate an excess of indium in the $CuInS_2$ particles. This contrasts with numerous studies that reported an excess of copper for most other synthetic methods[3,11,13,14,18,21−23,26,50,51] which resulted in the formation of a p-type $CuInS_2$, and furthermore a Cu_2S layer

(49) Arici, E.; Sariciftci, N. S.; Meissner, D. *Adv. Funct. Mater.* **2003**, *13* (2), 165–171.
(50) John, T. T.; Mathew, M.; Kartha, C. S.; Vijayakumar, K. P.; Abe, T.; Kashiwaba, Y. *Sol. Energy Mater. Sol. Cells* **2005**, *89*(1), 27–36.
(51) Marsillac, S.; Zouaghi, M. C.; Bernede, J. C.; Ben Nasrallah, T.; Belgacem, S. *Sol. Energy Mater. Sol. Cells* **2003**, *76*(2), 125–134.

was often formed at the surface of the particles.[1] To obtain an n-type semiconductivity, a chemical treatment using KCN[52] or an electrochemical treatment[53,54] was needed to reduce the excess of copper, but this leads to the formation of a In_2S_3 layer at the surface.[1] For example, electrodeposition methods[15−17] provides p-type semiconductivity (with a 20 to 40% excess of copper), even if a solution rich in indium is used. A colloidal method using hexanethiol as a ligand[31] resulted in n-type $CuInS_2$ particles with 8% excess of indium. In this present work, using a metal:TPP ratio of 1:3 and a double stoichiometric excess of sulfur, an excess of indium between 4 and 11% was obtained in the bulk of the material, indicating an improved control of the $CuInS_2$ stoichiometry. However, as pointed out by solid-state Raman spectroscopy, a CuAu phase, less efficient for the photovoltaic effect, is also present.

Electrochemical Impedance Spectroscopy. $CuInS_2$ particles synthesized in this work have a bandgap energy of 1.45 eV and semiconductors with E_g values between 1.1 and 1.7 eV are very sensitive to the photocorrosion and photopassivation processes in aqueous solutions.[55,56] As shown by Gerischer and Goberecht[57] for CdSe in aqueous electrolytes, the photogenerated holes that do not react fast enough with the reduced species of the redox couple corrode the semiconductor, which then gets dissolved in water. To prevent photocorrosion, two organic redox couples dissolved in nonaqueous media were used in this work.

EIS measurements were carried out on a film made of $CuInS_2$ particles annealed for 3 h at 450 °C. These measurements yield the type of semiconductivity, the majority charge carrier density (n_d) and the Fermi level of the semiconductor ($E_{F,sc}$), which is equal to the flatband potential (V_{FB}) in the dark. The measurements were done in the dark and at room temperature using the two different electrolyte solutions described previously, with TBAP used as a supporting electrolyte (0.3 M). Under conditions of concentrated electrolyte, the semiconductor space-charge capacitance (C_{sc}) is determined, for each applied potential, from the capacitive zone of the Nyquist diagrams ($-Z_{im}$ vs Z_{real}) using eq 4:

$$C_{sc} = \frac{1}{2\pi f |Z_{im}|} \qquad (4)$$

where $2\pi f$ is the angular frequency corresponding to the Z_{im} value, the imaginary component of the impedance. An overlay of typical Nyquist diagrams obtained for different potentials using the electrolyte containing the T^-/T_2 redox couple is illustrated in the Supporting Information S3.

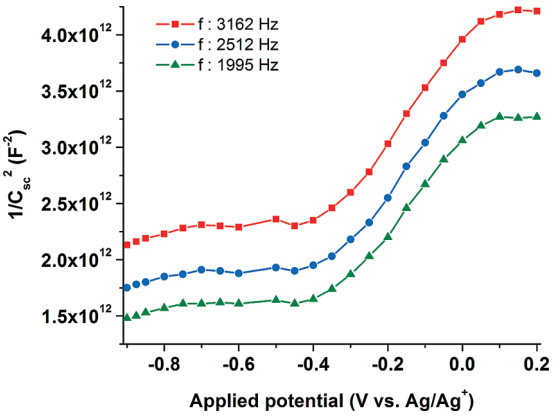

Figure 8. Mott−Schottky plots, obtained in the dark, at room temperature and at three frequencies, of a $CuInS_2$ electrode immersed into an acetonitrile solution containing the T^-/T_2 redox couple. The film is made of $CuInS_2$ particles annealed at 450 °C for 3 h under vacuum.

For a given frequency, the variation of $1/C_{sc}^2$ with the applied potential was plotted. Figure 8 shows Mott−Schottky plots obtained at three frequencies (1995, 2512, and 3162 Hz) for the T^-/T_2 redox couple. The same procedure was done for the G^-/G_2 redox couple. The Mott−Schottky equation is given by

$$\frac{1}{C_{sc}^2}(F^{-2}) = \left(\frac{2}{e\varepsilon_r\varepsilon_o n_d A^2}\right)\left(V - V_{FB} - \frac{kT}{e}\right) \qquad (5)$$

where e is the electron charge, ε_r is the relative permittivity (dielectric constant) of $CuInS_2$ (ε_r: 11),[58] ε_o is the vacuum permittivity, n_d is the majority charge carrier density, V_{FB} is the flatband potential, A is the electrochemically active surface area (3.7 cm^2), k is the Boltzmann constant, and T is the absolute temperature (295 K).

The positive slope of the curves between 0 and −0.3 V vs Ag/Ag^+, shown in Figure 8, indicates an n-type semiconductivity, in agreement with the EDX, ICP-AES, and XPS analyses (In/Cu ratio > 1). The flatband potentials and the majority charge carrier densities were calculated, respectively, from the intercept of the straight lines at $1/C_{sc}^2 = 0$ and from their slope. Figure 8 shows that the curves depend on the frequency. For both electrolytes, data corresponding to the curve obtained at the highest frequency (3162 Hz) were used. Indeed, high frequencies minimize the effect of surface states which are associated with surface defects and possibly adsorbed ions. These surface states may interfere with the impedance measurements if their relaxation time is lower than $1/f$. As shown in Table 3, $CuInS_2$ is characterized by a V_{FB} value of −0.55 V vs NHE with the T^-/T_2 redox couple, which corresponds to a semiconductor Fermi level ($E_{F,sc}$) of −3.95 eV. With the G^-/G_2 redox couple, a V_{FB} value of −0.86 V vs NHE is obtained, which corresponds to an $E_{F,sc}$ value of −3.64 eV. The semiconductor majority charge carrier densities are approximatively 4.1×10^{18} cm^{-3} and 1.8×10^{18} cm^{-3} with the redox couples T^-/T_2 and G^-/G_2, respectively. It has been

(52) Scheer, R. *Trends Vac. Sci. Technol.* **1997**, *2*, 77–112.
(53) Wilhelm, T.; Berenguier, B.; Aggour, M.; Kanis, M.; Lewerenz, H. J. *C. R. Chim.* **2006**, *9*(2), 294–300.
(54) Berenguier, B.; Lewerenz, H. J. *Electrochem. Commun.* **2006**, *8*(1), 165–169.
(55) Nozik, A. J. *Annu. Rev. Phys. Chem.* **1978**, *29*(1), 189–222.
(56) Wrighton, M. S. *Acc. Chem. Res.* **1979**, *12*(9), 303 –310.
(57) Gerischer, H.; Goberecht, J. *Ber. Bunsen-Ges.* **1978**, *85*(5), 520–522.
(58) Cattarin, S.; Dietz, N.; Lewerenz, H. J. *J. Electrochem. Soc.* **1994**, *141*(5), 1095–1099.

Table 3. Values of the Redox Potential (E_{redox}) and Fermi Level ($E_{F,el}$) of the T^-/T_2 and G^-/G_2 Redox Couples and Majority Charge Carrier Densities (n_d), Flatband Potentials (V_{FB}) and Fermi Levels ($E_{F,sc}$) of $CuInS_2$ Film Made of Particles Annealed at 450 °C for 3 h under Vacuum in Contact with the Redox Couples

redox couple	E_{redox} (V vs NHE)	$E_{F,el}$ (eV)	frequency (Hz)	n_d (cm^{-3})	V_{FB} (V vs NHE)	$E_{F,sc}$ (eV)
T^-/T_2	0.01	−4.51	3162	4.12×10^{18}	−0.55	−3.95
G^-/G_2	0.03	−4.53	3162	1.83×10^{18}	−0.86	−3.64

previously reported that $Cu_{0.99}InS_{1.96}$ electrodeposited on a titanium substrate gave an $E_{F,sc}$ value of −4.05 eV when the film was immersed into a DMF−DMSO (60:40 (vol%/vol%)) solution containing 10 mM HT, 1 mM T_2, and 0.2 M TBAP.[16] The $E_{F,sc}$ value determined in this work with the same T^-/T_2 redox couple is close to that value. On the other hand, the majority charge carrier densities are lower than the value of 4×10^{19} cm^{-3} associated with the electrodeposited $Cu_{0.99}InS_{1.96}$ film,[16] which was considered as a metalized semiconductor.

By using eqs 6, 7, and 8, the conduction and valence band edge energies, respectively E_c and E_v, can be calculated:

$$E_c - E_{F,sc} = \frac{-kT \ln\left(\frac{n_d}{N_c}\right)}{e} \quad (6)$$

where N_c is the conduction band effective density of states given by eq 7:

$$N_c = 2\left(\frac{2\pi m_e^* kT}{h^2}\right)^{3/2} = 2.5 \times 10^{19}\ cm^{-3} \quad \text{at} \quad 25\ °C \quad (7)$$

where m_e^* represents the electron effective mass, taken in a first approximation equal to the electron mass, m_o, and h is the Planck constant.

$$E_v = E_c - E_g \quad (8)$$

The $CuInS_2$/electrolyte energy level diagrams are depicted in Figure 9. The T^-/T_2 and G^-/G_2 redox potentials were measured equal to 0.01 and 0.03 V vs NHE, respectively, using a platinum working electrode. On the vacuum scale, the electrolyte Fermi levels ($E_{F,el}$) are −4.51 eV and −4.53 eV, respectively. As shown in Figure 9, in both cases, $E_{F,el}$ lies between E_c and E_v, which is needed for the oxidation of T^- or G^- by the photogenerated holes (under illumination) to occur. The nature of the redox couple affects the energy difference between $E_{F,el}$ and E_v, which is 0.77 eV with T^-/T_2 and 0.49 eV with G^-/G_2. This implies that there is a better overlap of the G^- filled energy states (reduced species) with the $CuInS_2$ valence band, leading to an expected more efficient electron transfer under illumination. As seen previously, the nature of the redox couple also affects $E_{F,sc}$, going from −3.95 eV (T^-/T_2) to −3.64 eV (G^-/G_2). The theoretical open-circuit photovoltage (V_{oc}) delivered by an electrochemical photovoltaic cell is given by the energy

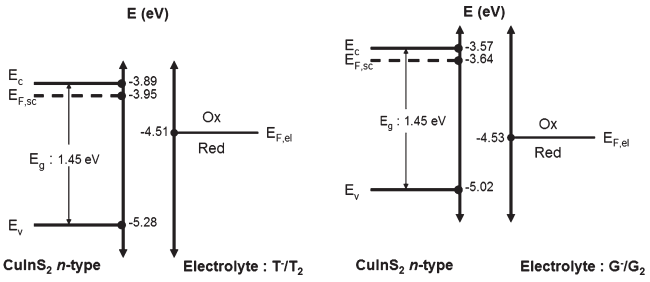

Figure 9. Energy level diagrams of a film of $CuInS_2$ immersed in two different electrolyte solutions: 100 mM T^-/10 mM T_2 in acetonitrile containing 0.3 M TBAP and 37.5 mM G^-/ 12.5 mM G_2 in EC-DMC containing 0.3 M TBAP.

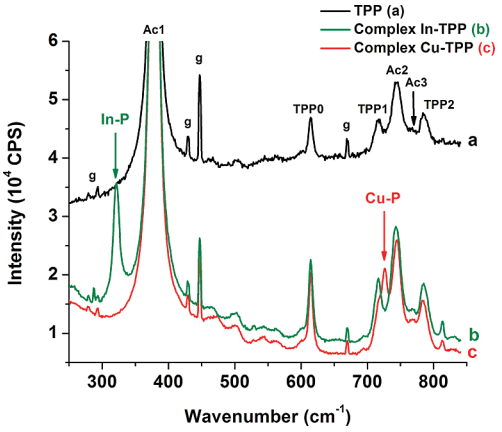

Figure 10. Raman spectra of (a) a 0.125 M TPP solution in acetonitrile, (b) a 0.115 M In-TPP complex solution in acetonitrile, and (c) a 0.115 M Cu-TPP complex solution in acetonitrile. The acquisition time is 80 s. (g) Raman vibration of the glass vial: Ac, Raman vibration of acetonitrile; TPP, Raman vibration of the TPP molecule.

difference between $E_{F,sc}$ and $E_{F,el}$. Thus, we can estimate V_{oc} values of 0.56 and 0.89 V, respectively, when using the T^-/T_2 and G^-/G_2 redox couples in the device. Therefore, it may be concluded that the G^-/G_2 redox couple should give a more efficient device (greater photocurrent and photovoltage).

In Situ Raman Spectroscopy. The surface analysis showed that indium is predominant at the surface of the particles. This observation suggests that copper and indium do not have the same reactivity toward hexamethyldisilathiane. Moreover, unlike most synthetic methods, the method used in this work provides n-type semiconductive particles (excess of indium in the bulk). In situ Raman spectroscopy measurements were thus carried out to investigate the reaction mechanism of the formation of the particles. The experiment consisted in monitoring the variation of the bands related to the reactants Cu−P and In−P bonds during the formation of the particles. Figure 10 shows the Raman reference spectra of solutions of TPP, Cu-TPP, and In-TPP in acetonitrile between 250 and 850 cm^{-1}. Throughout the entire spectrum (from 250 to 3200 cm^{-1}), only two differences have been observed between the metal-TPP spectra and the TPP spectrum: one peak at 321.5 cm^{-1} on the In-TPP spectrum and one peak at 726.8 cm^{-1} on the Cu-TPP spectrum. These peaks were assigned to the In−P and the Cu−P bonds, respectively. The Raman spectrum of the solution of

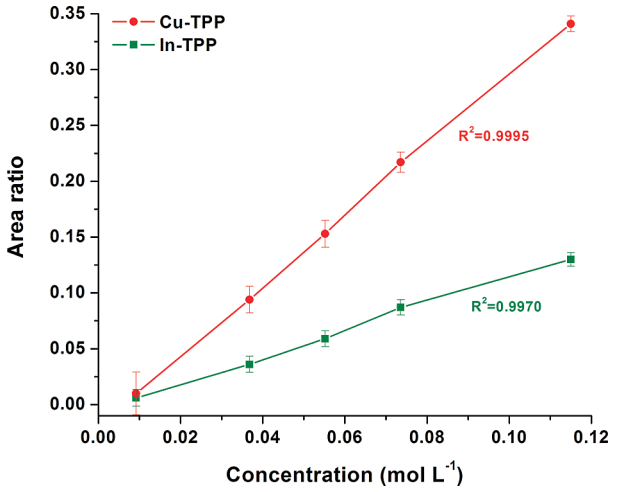

Figure 11. Graph of the Raman ratios In−P/Ac1 and Cu−P/Ac2 as a function of Cu-TPP and In-TPP concentration.

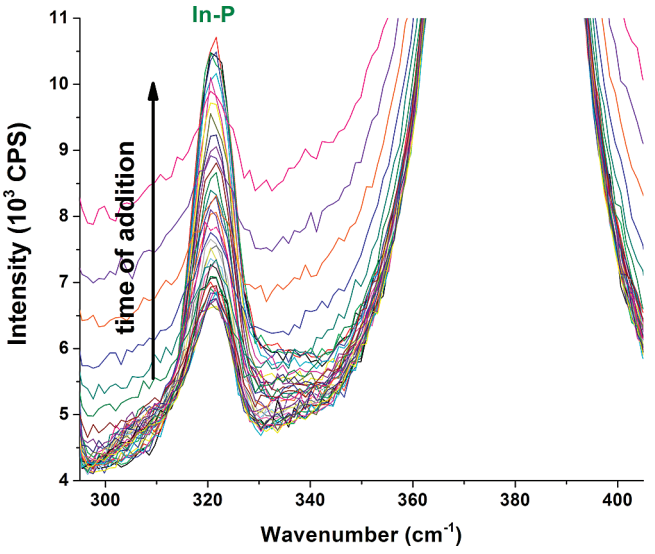

Figure 12. Variation of the In−P peak of a 0.0575 M In-TPP and Cu-TPP solution during the addition of a 0.1138 M hexamethyldisilathiane solution in acetonitrile (0.08 mL min^{-1}).

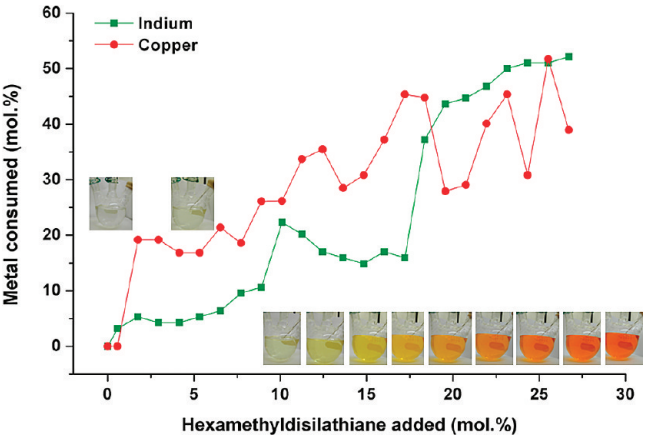

Figure 13. Graphs of the consumed concentration of indium and copper in mol % as a function the mol % of hexamethyldisilathiane (0.1138 M) added at a rate of 0.08 mL min^{-1}.

hexamethyldisilathiane in acetonitrile shows that the molecule exhibits three peaks between 250 and 850 cm^{-1}: 437.5 cm^{-1}, 639.3 cm^{-1}, and 696.0 cm^{-1} (see Supporting Information S4). Since acetonitrile is the solvent, the intensities of its peaks do not change during the reaction. Hence, the acetonitrile peaks near the In−P and Cu−P peaks were used as reference. The Ac1 peak at about 378.9 cm^{-1} in Figure 10 was used to quantify the In−P peak (ratio In−P/Ac1), and the Ac2 peak at about 744.1 cm^{-1} was used to quantify the Cu−P peak (ratio Cu−P/Ac2). Calibration curves were done to verify that the ratios In−P/Ac1 and Cu−P/Ac2 were proportional to the concentration of In-TPP and Cu-TPP. Figure 11 shows the calibration curve for a concentration range going from 0.009 to 0.115 M. It was then possible to follow the variation of these ratios as a function of time during the formation of the $CuInS_2$ particles and to relate them to reactant reaction.

Figure 12 shows the evolution of the intensity of the In−P peak of a solution containing 0.0575 M In-TPP and Cu-TPP while the hexamethyldisilathiane solution (0.1138 M in acetonitrile) was added at a rate of 0.08 mL min^{-1}. The evolution of the Cu−P peak is shown in the Supporting Information S5. With time, the relative intensity of the peaks decreases, which means that the In−P and Cu−P bonds are broken while In−S and Cu−S bonds are formed. At one point, it was not possible to follow further the peak intensities because the particles became too big which increased the light scattering and the background noise. It is important to note that no hexamethyldisilathiane peaks were observed during the reaction, which means that it reacted immediately upon addition.

Figure 13 shows the disappearance of In−P and Cu−P bonds as a function of the sulfur addition. Colloidal growth is a multiple-step process: the nucleation and the growth which consume metal ions, followed by aggregation of the particles where no metal ions are consumed. At the beginning of the reaction, the copper reagent is quickly consumed compared to the indium reagent which is almost not consumed. When 9 mol % of the hexamethyldisilathiane (~double excess) was added, the copper reactant has been consumed about three times faster than the indium one. At this point, the solution is still colorless. This first step is thus the formation of a soluble and colorless Cu(I)-S precursor with the sulfur source, which probably leads to the formation of Cu_2S nucleation sites. This has already been observed by Connor et al.[59] for the synthesis of $CuInS_2$ nanorods via the formation of a Cu_2S phase prior to $CuInS_2$ formation. During the second step, between 9 and 20 mol % of the hexamethyldisilathiane added, while copper is still being consumed, the consumption rate of indium started to increase. At this point the solution turned yellowish/light-orange, which is related to the growth of $CuInS_2$ particles. This second step corresponds to the indium insertion into the Cu(I)-S precursor to convert Cu_2S into $CuInS_2$, and then $CuInS_2$ continues to grow. After 20 mol % of the hexamethyldisilathiane

(59) Connor, S. T.; Hsu, C.-M.; Weil, B. D.; Aloni, S.; Cui, Y. *J. Am. Chem. Soc.* **2009**, *131*(13), 4962–4966.

was added, it is not possible to follow the disappearance of the Cu−P peak anymore because of its low intensity and because of the fact that the $CuInS_2$ particles became too big causing important scattering that leads to an intense background. This limited the extent of our kinetic studies. This in situ study, nevertheless, demonstrated that copper has a higher reactivity than indium with sulfur when the metals are complexed with TPP. The higher indium content at the surface of the particles is thus explained by the fact that it is the last one to react, so the particles are covered with an indium rich phase.

According to the calibration curve, for a concentration of 0.0575 M, the starting In−P/Ac1 and Cu−P/Ac2 ratios should be 0.063 and 0.161, respectively. Experimentally, for the solution of 0.0575 M In-TPP and Cu-TPP, the Cu−P/Ac2 ratio is 0.170, very close to the prediction. However, the In−P/Ac1 ratio is 0.095, about one-third greater than the expected value. This means that more In−P bonds are present in the Cu-TPP and In-TPP mixture than into the In-TPP solution. We assign the ratio of 0.063 to a complex with two In−P bonds whereas the ratio of 0.095 is assigned to a complex with three In−P bonds. This result explains a previous observation done during the synthesis optimization process. When a ratio of one indium for two TPP was used to prepare the In-TPP complex, particles with an excess of copper were always obtained, whereas the use of a ratio of one indium for three TPP provided $CuInS_2$ particles with an excess of indium. The stoichiometry of the Cu-TPP and In-TPP complexes are not well-known. The two ligands TPP and PPh_3 are very close chemically; in the literature, Cu(I)-TPP and Cu(I)-PPh_3 complexes with Cl^- or ClO_4^- as counterions have been identified.[60−62] With ClO_4^- as a counterion, the complexes $[Cu(TPP)_4]^+$ (soluble in chloroform and TPP) and $[Cu(PPh_3)_4]^+$ (soluble in chloroform only) were identified. With Cl^- as a counterion, only three PPh_3 ligands are needed: $[Cu(PPh_3)_3]^+$. Equivalent complexes, with TPP as a ligand, have not been reported in the literature. In the case of indium, only one complex In(III)-PPh_3 has been found in the literature with Cl^- as a counterion and two PPh_3 ligands: $In(PPh_3)_2Cl_3$.[63,64] Our experiments do resolve this issue, but we did observe that using an In:TPP ratio of three results in an excess of indium in the stoichiometry of the $CuInS_2$ particles, making them a better candidate as solar cell material.

(60) Reichie, W. T. *Inorg. Chim. Acta* **1971**, *5*, 325–332.
(61) Nilsson, K. B.; Persson, I. *Dalton Trans.* **2004**, *9*, 1312–1319.
(62) Pike, R. D.; Starnes, W. H.; Carpenter, G. B. *Acta Crystallogr., Sect. C: Cryst. Struct. Commun.* **1990**, *C55*, 162–165.
(63) Veidis, M. V.; Palenik, G. J. *Chem. Commun.* **1969**, 586–587.
(64) Carty, A. J.; Tuck, D. G. *J. Chem. Soc. A* **1966**, 1081–1087.

Conclusion

In situ Raman spectroscopy measurements provided insights into the growth mechanism of $CuInS_2$ particles prepared from a modified Czekelius's method.[29,30] We demonstrated that the reactivity of copper with hexamethyldisilathiane is faster than the indium one. It explains the excess of indium at the surface of the particles and also the importance of the ligand into modulating the reactivity of the metallic ions with the sulfur compound. The detailed characterization of the particles supports the proposed growth mechanism. EDX, ICP-AES and XPS revealed $CuInS_2$ particles with an excess of indium of about 10% in the bulk and 40% at the surface (annealed at 450 °C); also, annealing the particles under vacuum largely decreased the organic. Solid state Raman spectroscopy performed on the powder identified CH and CuAu structures, and UV−visible spectroscopy showed that $CuInS_2$ possesses a bandgap energy of 1.45 eV. The electrochemical analyses demonstrated that this synthetic method produces particles with an n-type semiconductivity. Moreover, the two organic redox couples used for the EIS measurements (T^-/T_2 and G^-/G_2) provided $CuInS_2$ Fermi levels of −3.95 eV and −3.64 eV and majority charge carrier densities of 4.1×10^{18} and 1.8×10^{18} cm^{-3}, respectively. G^-/G_2 redox couple showed a better overlap of the reduced species filled energy states with the $CuInS_2$ valence band edge (expected greater photocurrent) and a higher theoretical open-circuit photovoltage (0.89 V).

Acknowledgment. The authors acknowledge the financial support of the Natural Sciences and Engineering Research Council of Canada (NSERC), the Fonds québécois de la recherche sur la nature et les technologies (FQRNT), the Institut National de la Recherche Scientifique (INRS). and the Université du Québec à Montréal (UQÀM).

Supporting Information Available: The XPS survey spectrum of the $CuInS_2$ particle, the structure of the two redox couples used for the electrochemical measurements, the Nyquist diagrams obtained for different applied potentials for a film made of $CuInS_2$ particles, the Raman spectra of a solution of hexamethyldisilathiane, and the graph of the variation of the Cu−P peak during the addition of a hexamethyldisilathiane solution in acetonitrile (PDF). This material is available free of charge via the Internet at http://pubs.acs.org.